PERGAMON

International Journal of Heat and Mass Transfer 45 (2002) 465–482

International Journal of HEAT and MASS TRANSFER

www.elsevier.com/locate/ijhmt

Experimental study of the convective heat transfer from in-line and staggered configurations of two wall-mounted cubes

E.R. Meinders [a,*], K. Hanjalić [b]

[a] *Philips Research Laboratories, Materials and Process Technology, Prof. Holstlaan 4, 5656 AA, Eindhoven, Netherlands*
[b] *Faculty of Applied Physics, Delft University of Technology, P.O. Box 5046, 2600 GA, Delft, Netherlands*

Received 10 February 2001; received in revised form 25 May 2001

Abstract

The paper reports on the experimental investigation of the effects of the relative obstacle position on the convective heat transfer from a configuration of *two* wall-mounted cubes located in a fully developed turbulent channel flow. Both in-line and staggered arrangements were studied for various streamwise (S_x/H) and spanwise (S_z/H) distances. Distributions of the local heat transfer coefficient (h) were obtained from infrared thermography and local convective heat flux analyses. Laser Doppler anemometry measurements and flow visualisations were performed to document the flow and turbulence fields around the cubes. The results showed a large variation in the distribution of the local convective heat transfer for the various in-line and staggered configurations studied. While the in-line arrangements were featured by symmetric flow pattern and heat transfer distributions, the staggered arrangements showed distinct asymmetric pattern for certain combinations of S_x/H and S_z/H. Flow reattachment caused typically a monotonic decay of the convective heat transfer. On the other hand, flow separation caused distinct heat transfer extrema at the cube faces. In addition, the effect of vortex shedding on the convective heat transfer of the downstream cube was studied with a fast-responding heat flux sensor. Despite distinct variation in the distribution of the time-averaged heat transfer coefficient, the cube-averaged heat transfer coefficients appeared to be independent of the relative placement of the two cubes.

1. Introduction

Printed electronic circuit boards typically consist of arrays of protruding aerodynamic bluff components. The temperature control of critical components is essential for optimum board and system performance since local overheating is still a major cause of technical failure. The avoidance of component damage relies on accurate predictions of the total conjugate heat transfer. Among the different modes of heat transfer, the local convective heat transfer during operation is still difficult to determine accurately. It strongly depends on the local flow structures and relies therefore on the prediction of the local flow pattern. Although the low velocities and small length scales encountered in electronic cabinets correspond to low Reynolds numbers, the flow is usually highly complex, three-dimensional, transitional or turbulent. The local structures of the mean flow, such as flow separation, reattachment and recirculation, and the corresponding high turbulence fields, make an accurate determination of the distributions of the local convective heat transfer a difficult task.

Insight into the heat transfer mechanisms can be obtained from studies with model configurations. The tandem arrangement of two cubes in a fully developed turbulent channel flow is such a suitable test case since it involves much of the mentioned generic flow features. In addition, the aerodynamic interference between the two cubes gives rise to quasi-periodic phenomena which may lead to an augmentation or degradation of the local and average convective heat transfer.

The vortex shedding at the lateral faces of the leading cube causes periodic flow instabilities in its wake that may either be attenuated or amplified by the interaction

* Corresponding author. Tel.: +31-40-27-450-70; fax: +31-40-27-450-02.

E-mail address: erwin.meinders@philips.com (E.R. Meinders).

0017-9310/02/$ - see front matter
PII: S0017-9310(01)00180-6

Nomenclature

D	channel width (m)
h	local heat transfer coefficient (W m^{-2} K^{-1})
$\bar{h}$	averaged heat transfer coefficient (W m^{-2} K^{-1})
f	frequency of vortex shedding (Hz)
H	cube rib (mm)
Re_H	Reynolds number $Re = u_B H v^{-1}$
P	power supply (W)
St	Strouhal number ($St = fHu_B^{-1}$)
S_x	streamwise distance between cubes (m)
S_z	spanwise distance between cubes (m)
k	turbulent kinetic energy ($k = 0.75(\overline{u'^2} + \overline{v'^2})$) (m^2 s^{-2})
$\mathrm{d}T/\mathrm{d}n$	temperature gradient at surface cube (K m^{-1})
T_s	surface temperature (K)
T_{in}	inlet temperature (K)
$\overline{u'^2}$	Reynolds normal stresses (m^2 s^{-2})
u_B	bulk velocity (m s^{-1})
u_∞	free stream velocity (m s^{-1})
$\overline{v'^2}$	Reynolds normal stresses (m^2 s^{-2})
x, y, z	coordinates

Greek symbols

λ	thermal conductivity (W m^{-1} K^{-1})
v	kinematic viscosity (m^2 s^{-1})
$\phi''_{\mathrm{cond}}\|_s$	conductive heat flux at surface (W m^{-2})
ϕ''_{conv}	convective heat flux (W m^{-2})
ϕ''_{rad}	radiative heat flux (W m^{-2})

with the flow field of the downstream cube. The distance between the cubes is an important parameter affecting this time-dependent flow behaviour. Flow interference may occur over a range of distances. When the spacing approaches zero, the mutual flow interaction vanishes and the resulting obstacle is considered to be an extended cube of doubled size. In the opposite limit, when the distance approaches infinity, flow interference also vanishes and the cubes behave like two aerodynamically independent cubes. The convective heat transfer from both the leading and downstream cubes may either be intensified or decreased by the flow field interaction. The oscillatory behaviour of the reattaching flow may locally augment the convective heat transfer. On the other hand, flow interference may cause heat to be convected away slowly in areas in which the time-mean velocities are low, which will lead to hot spots. Vortex shedding from single wall-mounted rectangular obstacles is reported in the literature. Martinuzzi and Tropea [1] have published dimensionless Strouhal numbers ($St = fH/u_B$, where u_B is the bulk velocity, f is the predominant frequency and H is the obstacle size) for single wall-mounted bluff bodies. Further, a series of papers have been published on the aerodynamic interaction between two suspended infinitely long rectangular cylinders [2–4]. The investigation of Luo and Teng [5] of the aerodynamic forces acting on the downstream square cylinder of an in-line tandem arrangement (cylinder side dimension D) showed the existence of a critical spacing of $S/H = 3$, for which the shedding frequency was minimum. For smaller distances, the shear layer separating from the leading cylinder reattached on the second cylinder and vortex shedding was detected only downstream of the latter cylinder. For larger spacings, vortex shedding was detected behind both cylinders.

Measurements of the convective heat transfer distributions on a single cube, an in-line row of nine heated cubes and cubes placed in a spatially periodic matrix arrangement have been discussed in previous publications of the authors [6–9]. These studies showed that large spatial gradients existed in the heat transfer coefficient which were attributed to the local flow structure around the cubes. These test cases served primarily to analyse the local heat transfer phenomena and make analogy with the local flow structures. An extensive literature review of previous work on heat transfer and flow field analysis of wall-mounted cubes in turbulent channel flow was also given in these publications. The objective of the present work is to analyse the local convective heat transfer of in-line and staggered arrangements of *two* wall-mounted cubes at a range of different longitudinal and lateral spacings. To adequately interpret the heat transfer coefficient distributions, the local flow structures around the two cubes were analysed via laser Doppler anemometry measurements and visualisation studies. Distributions of the local convective heat transfer were obtained from infrared thermography and local convective heat flux analyses. The effect of vortex shedding on the heat transfer of the downstream cube was studied with a fast-responding flush-mounted heat flux sensor.

2. Experimental details

2.1. Set-up

A tandem configuration placed on one of the walls of a rectangular section of a closed wind tunnel is considered for most of the experimental work discussed here. The flow was fully developed in the test section, which was demonstrated from measured velocity profiles. The bulk velocity u_B was obtained from integrated velocity profiles and was used to define a Reynolds number

$Re_H = Hu_B/v$, where H is the cube size and v is the kinematic viscosity. All measurements in the fully developed channel flow were performed at a bulk velocity of 3.9 m s^{-1}, which corresponds to a Reynolds number of $Re_H = 3900$. The cube size was $H = 15$ mm and the channel height D was 51 mm, thus giving a channel-height-to-cube-height ratio of $D/H = 3.4$. Both the streamwise and spanwise centre-to-centre distances (S_x/H and S_z/H) were varied. Sketches of the side and plan view of the test-configuration are given in Fig. 1. x, y and z denote, respectively, the streamwise, the normal and the spanwise directions.

Some additional frequency measurements were performed in a developing turbulent boundary layer flow with cubes of size $H = 25$ and 50 mm at a Reynolds number of $Re_H = 10{,}750$ and 21,500, respectively (the Reynolds number was based on the free stream velocity U_∞).

2.2. Flow measurement

The flow around the cubes was visualised with, among others, the oil-film technique. This technique is based on the removal and the accumulation of the visualisation pigment (graphite) in a tracer mixture of jet fuel and low-transmission oil. The time-averaged structure of the flow immediately above the surface is visualised in that way. The oil-film visualisations were performed at a somewhat higher Reynolds number, namely $Re_H = 7000$, but it was confirmed that the flow field was qualitatively similar to that at $Re_H = 3900$. The visualisations were primarily intended to qualitatively observe significant differences in wall streak pattern, when varying the distance between the cubes. A laser Doppler anemometer (LDA) was used to provide quantitative information of the mean flow and turbulence fields. Background information of the technical aspects of the LDA system, the data processing, the experimental uncertainty involved (e.g velocity bias, optical alignment, etc.), etc. is given in [7]. Here, it is only mentioned that the overall accuracy for the long-term averaged velocities and second-order moments were 5% and 10%, respectively. The frequencies associated with vortex shedding were obtained from the power density spectra of the velocity time traces measured with the LDA system. The frequency measurements for the tandem in the developing turbulent boundary layer were performed with a commercial hot wire anemometer (TSI). The frequencies are represented as the non-dimensionless Strouhal number. Considering the accuracies involved, the Strouhal number was evaluated within about 10% accuracy.

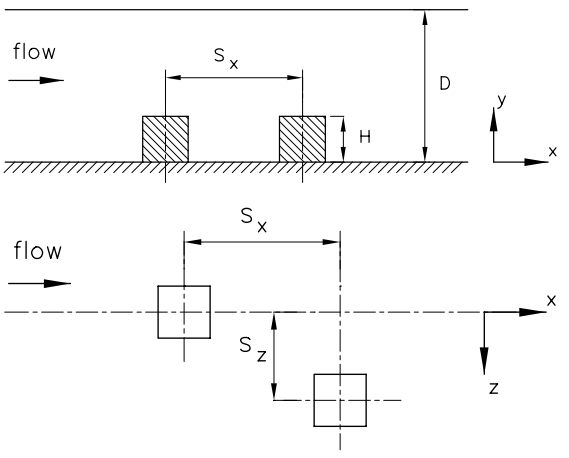

Fig. 1. Sketches of the side view (upper plot) and the plan view (lower plot) of the tandem arrangement of wall-mounted cubes in the channel.

2.3. Heat transfer

Distributions of the local convective heat transfer at the faces of the cubes were obtained from a three-dimensional heat flux analysis. The measurement cubes consisted of a 12 mm cubical copper core covered by a thin epoxy layer machined to 1.5 mm uniform thickness. A heat source was embedded in the copper core.

The surface temperature distribution of the cube was acquired using an infrared imaging system. The camera was mounted at a 45° scan angle to enable the measurement on the lateral faces of the cube without disturbing the air flow. A high temperature accuracy and high spatial resolution without losing depth of field were obtained by using an image restoration technique based on Wiener filtering. The two-dimensional optical transfer function, which is a characteristic of the used infrared imaging system, was measured and utilised in the Wiener restoration filter. An in-situ calibration was developed to account for miscellaneous environmental contributions to the total received radiosity by the camera. By utilising this in-situ calibration and infrared image restoration, the accuracy of the surface temperature measurements was improved to 0.4°C. This accuracy was confirmed with independent liquid crystal surface temperature measurements [10].

The high thermal conductivity of the copper core, in combination with the low thermal conductivity of the epoxy layer surrounding it, resulted in a uniform copper temperature. The infrared surface temperature distribution and the uniform copper temperature served as thermal boundary conditions to solve the three-dimensional heat diffusion equation in the epoxy layer. From the resolved temperature distribution, the local temperature gradient normal to the surface, $\partial T/\partial n$, was obtained which gives, together with the thermal conductivity of the epoxy substrate (λ), the local conductive heat flux at the surface of the cube. The local net radiative heat flux, ϕ''_{rad}, was approximated from the

Stefan–Boltzmann relationship using the surface temperature distribution, ambient temperatures (channel walls) and surface emissivity. The radiative heat flux correction was at maximum 10–15% of the conductive heat flow. A heat balance at the surface yields the local convective heat flux ϕ''_{conv} ($\phi''_{\mathrm{conv}} = \phi''_{\mathrm{cond}}|_{\mathrm{s}} - \phi''_{\mathrm{rad}}$) and thus the local heat transfer coefficient (h):

$$h = \frac{\phi''_{\mathrm{cond}}|_{\mathrm{s}} - \phi''_{\mathrm{rad}}}{T_{\mathrm{s}} - T_{\mathrm{in}}}, \tag{1}$$

where T_{s} and T_{in} are the local surface temperature and the reference inlet temperature, respectively.

The overall accuracy of the measured heat transfer coefficients is primarily determined by the uncertainty in the surface temperature distribution. Further, the thermal conductivity (measured to be $\lambda = 0.24 \pm 2\%$) and layer thickness of the epoxy layer are major contributors to the experimental accuracy. From a single-sample uncertainty analysis, an overall accuracy of about 10% is estimated. A complete discussion and evaluation of the developed method and measurement techniques are given in [7,10].

3. Velocity field, turbulence and flow structures

3.1. In-line tandem

The flow pattern around an in-line tandem of cubes can be inferred from the combined oil-surface imprints of the wall streaks, velocity vectors and streamline distribution in various cross-sections, shown in Figs. 2–6. The main feature is a horseshoe vortex formed upstream of the front face of the leading cube due to the adverse pressure gradient. The vortex is deflected downstream along the side faces of the upstream cube. The oncoming flow, separated from the leading side and top edges of the upstream cube, penetrated the inter-obstacle spacing and reattached on the channel floor at approximately 1.5 cube distances from the leeward face. The top and side vortices are due to flow separation at the leading edges. The flow reattachment in the inter-obstacle wake caused a second horseshoe vortex to develop in front of the downstream cube and leads to separation bubbles at the top and side faces of the downstream cube as well. The wake of both cubes is characterised by an arc-shaped vortex, confined by the side flow and the separating shear layer flowing over the top of the cubes.

These flow features can be traced back from the oil-film visualisation given in Fig. 2. The two horseshoe vortices in front of the cubes are identified from the bent pigment structure. The arc-shaped vortex in the wake of the leading cube is identified from the confocal pigment concentrations in Fig. 2. The pigment concentrations close to the leading side edges are caused by the side vortices. The smeared pigment pattern in the inter-obstacle reattachment region indicates the highly unsteady nature of the reattaching flow.

Velocity measurements of the flow around the first cube in the plane of symmetry $z/H = 0$, given in vector representation in Fig. 3, indicate the presence of the horseshoe vortex, the top vortex and the wake vortex. The presence of a second vortex upstream of the main horseshoe vortex can be inferred from the somewhat distorted flow upstream of the primary vortex. The corresponding increase in the turbulent kinetic energy, denoted as $k = 0.75(\overline{u'^2} + \overline{v'^2})$ and given in the lower plot in Fig. 3, is also indicative for the second vortex. Measurements of the time-averaged velocity field at $y/H = 0.5$ are given in Fig. 4. Only one half of the flow domain is shown since flow symmetry was verified with measurements. The velocity vectors clearly indicate the flow separation and the resulting vortex at the sides of the leading cube. The flow separation at the leading side

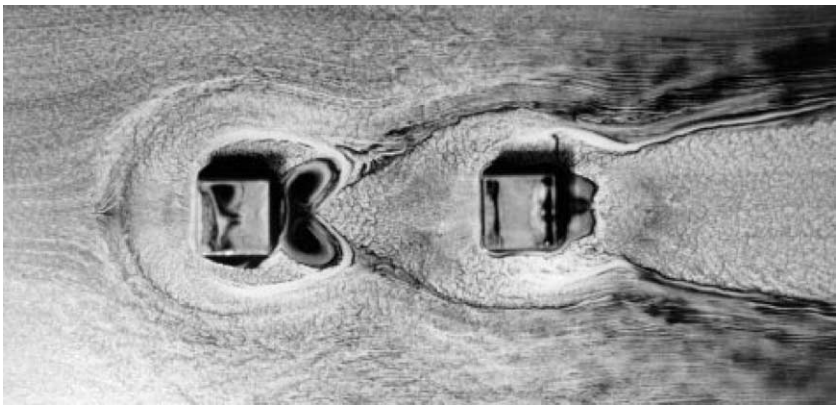

Fig. 2. Oil-film visualisation of the surface streak pattern of an in-line tandem arrangement of cubes with spacing $S_x/H = 4$ ($Re_H = 7000$).

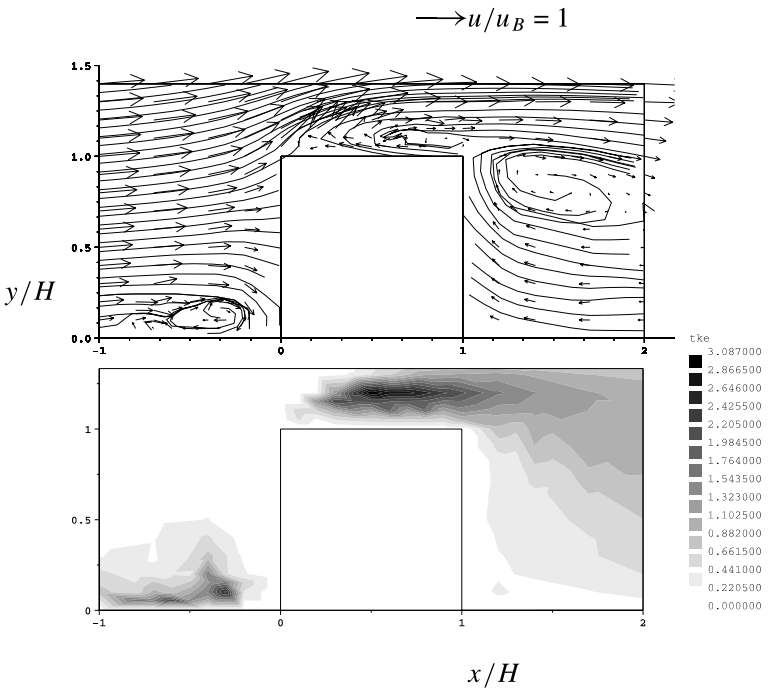

Fig. 3. Vector plot with streamlines and an iso-value plot of the turbulent kinetic energy in the symmetry plane $z/H = 0$ for the leading cube in the in-line tandem of cubes with $S_x/H = 4$ ($Re_H = 3900$).

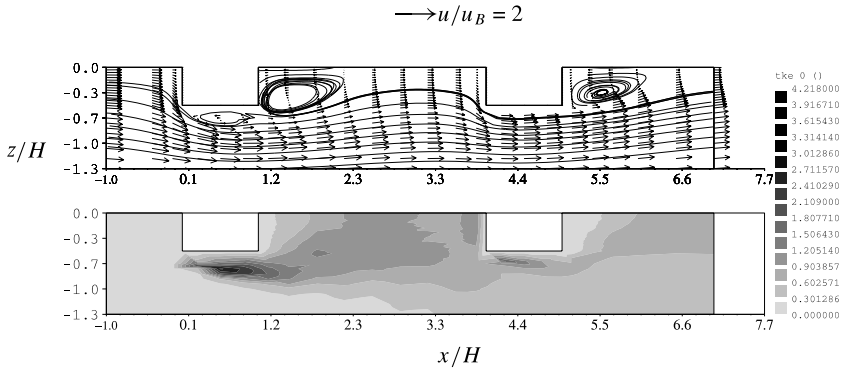

Fig. 4. Vector plot with streamlines and an iso-value plot of the turbulent kinetic energy in a plane parallel to the channel floor at $y/H = 0.5$ for the in-line tandem with spacing $S_x/H = 4$ ($Re_H = 3900$).

edge of the downstream cube can be deduced from the curvature of the streamlines following the flow outward the cavity. Arc-vortices are found in the wake of both cubes and their locations are in good agreement with the oil-film observations. The turbulent kinetic energy $k = 0.75(\overline{u'^2} + \overline{w'^2})$, given in Fig. 4, is quite high at the interface of the side vortex and the shear layers. It is further seen from the turbulent kinetic energy plot that the intermittent reattachment of the shear layer in the inter-obstacle spacing contributed significantly to the production of turbulence.

The most significant difference in flow structure for a reduced inter-obstacle space ($S_x/H = 2$) is the absence of flow reattachment at the channel floor between the cubes. Instead, the oncoming flow reattaches at the front side edges of the downstream cube, where it splits into a boundary layer flow along the sides of the downstream cube and a recirculation flow in the inter-obstacle cavity. The inter-obstacle space is then characterised by one recirculation, filling the entire gap. A cross-section of the flow at $y/H = 0.5$ is shown in Fig. 5. A further observation was that the flow in front of the leading cube is

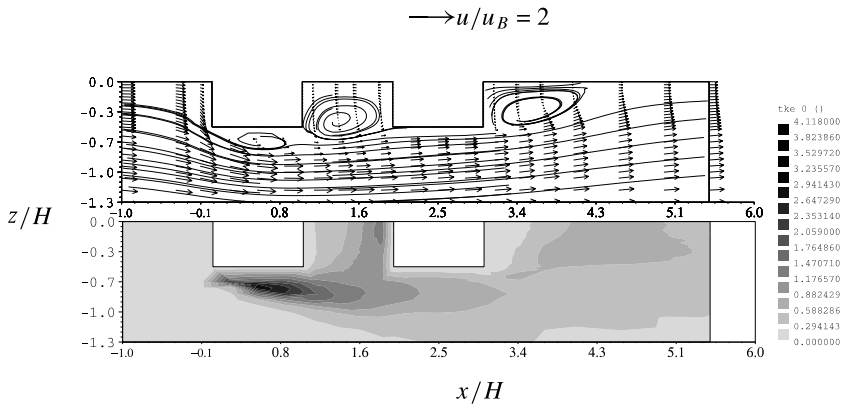

Fig. 5. Vector plot with streamlines and an iso-value plot of the turbulent kinetic energy in a plane parallel to the channel floor at $y/H = 0.5$ for the in-line tandem with spacing $S_x/H = 2$ ($Re_H = 3900$).

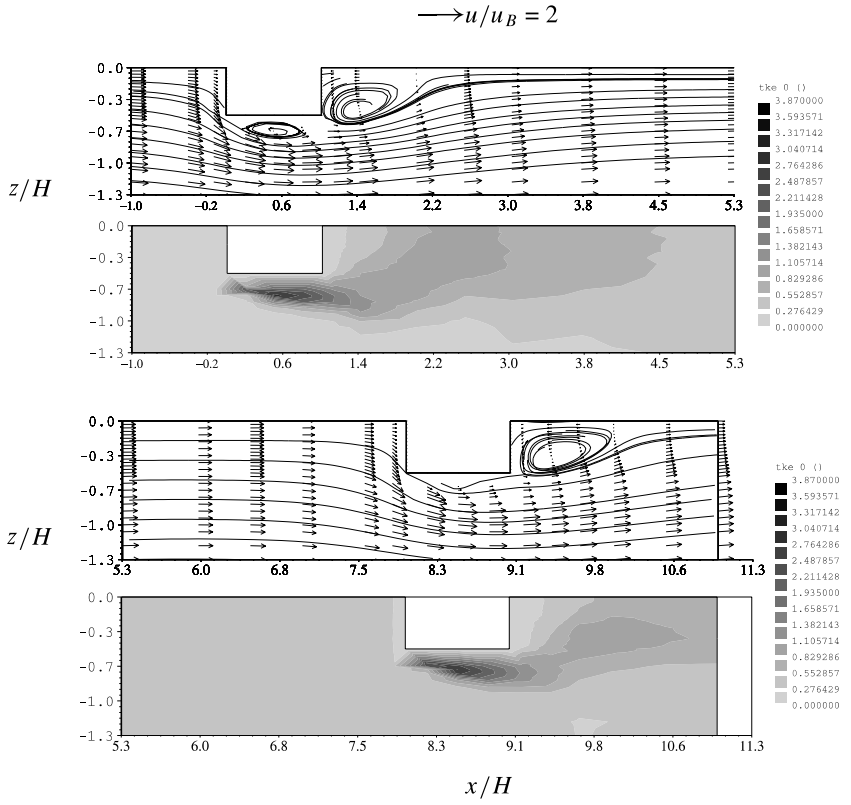

Fig. 6. Vector plots with streamlines and iso-value plots of the turbulent kinetic energy in a plane at $y/H = 0.5$ for the first (upper plot) and second (lower plot) cube in the in-line tandem with $S_x/H = 8$ ($Re_H = 3900$).

hardly affected by the change in streamwise distance. The flow clearly separates at the leading side edges of the first cube causing the pronounced separation vortices. The turbulent kinetic energy k, also given in Fig. 5, becomes maximum at the interface between the side vortices and adjacent shear flow. An intensification of the turbulence level also occurred in the downstream shear layer. Strong shearing and the quasi-periodic velocity fluctuations both contributed to the high turbulence levels.

The LDA results for the case with a larger streamwise distance, namely $S_x/H = 8$, are given in Fig. 6. The shear layer reattached at the channel floor in the inter-obstacle spacing at approximately $x/H = 2.5$. The flow around the leading cube is again characterised by the vortices at the side, the bound vortex at the top and the wake vortex. The relatively large distance between the cubes allowed the flow to recover in a time-averaged sense as is observed from the mean flow field after the flow reattachment at the channel floor. However, the upstream protrusion disturbed the flow, which led to a rather high level of the turbulence intensity as experienced by the downstream obstacle. The mean flow and turbulence fields around the downstream cube exhibit a large similarity with those around the upstream cube, but the recirculations are generally smaller.

3.1.1. Flow dynamics: vortex shedding

The frequencies associated with vortex shedding from the lateral faces of the cubes were determined from LDA measurements performed at stations in the wake of the leading cube. Typical stations were at $x/H = 1.2$–2, $y/H = 0.5$ and $z/H = 0.5$. Dimensionless wake frequencies in terms of the Strouhal number St, based on the bulk velocity, are given in Fig. 7 as a function of S_x/H. The results for the fully developed turbulent channel flow at $Re_H = 3900$, indicated with (○), show a minimum in the dominant frequency at a gap size of $S_x/H = 2.9$. The onset of vortex shedding activity was detected at $S_x/H = 2.4$. With increasing S_x/H, the shedding frequencies gradually converged to the value found for the infinite distance, a situation which corresponds to a single cube. The variation of S_x/H appeared to have a significant effect on the curvature of the shear layer separated from the leading edge of the upstream cube. For $S_x/H = 2$, it was found that the shear layer reattached at the leading edges of the downstream cube while flow reattachment at the channel floor at $x/H = 2.5$ was found for $S_x/H = 4$. From the flow visualisation observations made for $S_x/H = 3$ (not shown in this paper) it can be concluded that the shear layer reattaches at the lower edge of the windward face. Differences in the curvature caused the adverse pressure gradient in the cavity to be different, which consequently resulted in the observed minimum in the shedding frequency.

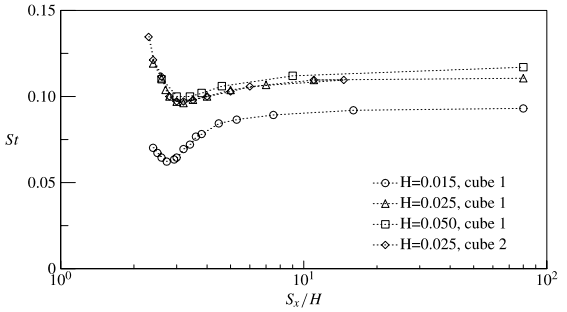

Fig. 7. Measured dominant wake frequencies of the leading cube as a function of S_x/H for the in-line tandem in fully developed turbulent channel flow ($H = 1.5$ cm: ○) and in a thin turbulent boundary layer ($H = 2.5$ cm: △; and $H = 5.0$ cm: □). The markers ◇ indicate the wake frequencies for the second cube.

The Strouhal numbers for the leading cube in a tandem arrangement placed in a thin turbulent boundary layer at $Re_H = 21{,}500$ are indicated with △ and □, for a cube size of, respectively, $H = 2.5$ and 5.0 cm. Although these measurements also show a minimum frequency at a gap size of $S_x/H = 3.0$–3.2, the Strouhal numbers are significantly higher than those for the fully developed channel flow ($Re_H = 3900$). The small shift in the critical distance, for which the shedding frequency becomes minimum, is most likely due to flow structure differences around the cube, for example the curvature of the separated shear layer. A minimum in frequency was also observed by Takeuchi and Matsumoto [2,3] who studied the interference between two square cylinders suspended in a uniform free stream. They found a critical gap space of $S_x/H = 3$. It is interesting to note that, despite totally different oncoming flow conditions being encountered, the agreement is remarkably good, suggesting that the mechanism of vortex shedding is mainly dominated by inviscid flow effects.

Non-dimensionalised shedding frequencies measured in the wake of the second cube (with $H = 2.5$ cm and $Re_H = 10,750$) are indicated with (◇) in Fig. 7. It is observed that the shedding frequencies in the wake of the first and the second cube are the same, at least within the experimental uncertainty in determining the shedding frequency. We note that the frequencies behind the two cubes were not measured simultaneously. Observed differences in the frequencies as seen in Fig. 7 are most likely due to experimental artifacts, for example duplicating S_x, between two separate experiments. These small differences are amplified in the vicinity of the critical region because of the strong sensitivity of the frequency to spacing. The similarity nevertheless indicates that the vortex shedding of both cubes is frequency locked. At the moment it is not clear if a phase shift exists between the two shedding mechanisms.

3.2. Off-axis tandem

While the long-term averaged flow field was symmetric in the in-line tandem cases, the results for the staggered arrangements were significantly asymmetric for some combinations of the streamwise and the spanwise distance. For either a large streamwise or spanwise distance, no significant asymmetry of the

long-term averaged flow field is expected and, therefore, these arrangements represent more or less the flow around a single cube. But for relatively small streamwise and spanwise distances, the flow will be significantly affected by the downstream staggered cube, which results in asymmetry of both the averaged flow pattern and the corresponding convective heat transfer.

For the interpretation of the off-axis results, we will distinguish between the inner and outer side face of the leading and of the downstream cube. The outer side face is the face pointing outwards from the tandem; both inner side faces (of the upstream and downstream cube) point to each other.

The first off-axis configuration discussed had a streamwise and spanwise distance of $S_x/H = 2$ and $S_z/H = 1$, respectively. An oil-film visualisation of the surface streak lines is given in Fig. 8. The horseshoe vortex in front of the leading cube can clearly be seen from the pigment pattern. The rather symmetric pigment traces in this upstream region suggest that the flow impinges perpendicularly on the front face. This flow symmetry can also be seen from the long-term averaged vector plot of the velocity field ($y/H = 0.5$) given in Fig. 9. The downstream off-axis obstacle caused an extra blockage effect which imposed additional flow resistance. While the separated side shear layer reattached at the outer side wall of the leading cube, thus causing a small side vortex close to the leading edge, the inner side face is covered entirely by a side vortex without flow reattachment at the back half of the face. This obviously is caused by the downstream cube blocking which causes the oncoming flow to be deflected towards the inner side face of the first cube. This caused a large recirculation and, therefore, the absence of flow reattachment at the back half of the side face. The flow accelerated through the corridor between the cubes. Since the flow was about 45° inclined with respect to the system centreline, it separated at the inner side face of the downstream cube and caused the rather large side vortex at this side face (see Fig. 9). Further, a big flow recirculation in the wake of the upstream cube resulted from the inclined oncoming flow. Instead of the arch-shaped vortex, as found for the symmetric flow cases, the wake was characterised by a one-centre wake vortex. The wake of the downstream cube exposed a one-centre recirculation as well.

From the oil-film visualisation it is seen that the extension of the horseshoe vortex, induced in front of the first cube, interacts with the vortex in front of the second cube. This caused a strong intensification of the turbulence production which subsequently may cause heat transfer enhancement.

High turbulence intensities were found at the interfaces between the side vortices and the shear layers for both cubes. Both the flow instabilities and strong shearing caused the large values of the turbulent kinetic energy in the shear layers and the free mixing layers behind the lateral faces of the cubes (see lower plot in Fig. 9). The vortices in the wake of both cubes are rather stable, as may be concluded from the low values of the turbulence intensity. The region in front of the cubes have the lowest level of k. Since the considered plane at $y/H = 0.5$ does not intersect with the horseshoe vortices found upstream of both cubes, an increased turbulence level as usually found in the horseshoe vortex is not visible from the plot.

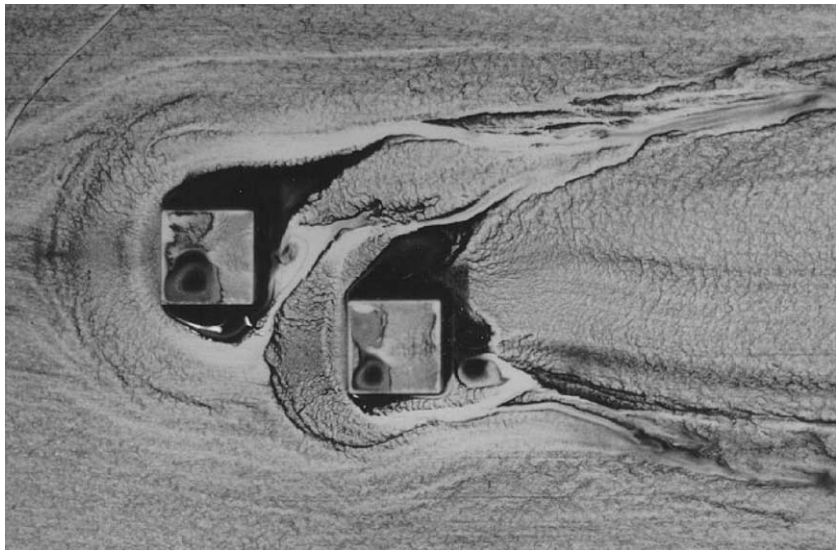

Fig. 8. Oil-film visualisation of the surface flow pattern of the staggered tandem with $S_x/H = 2$ and $S_z/H = 1$ ($Re_H = 7000$).

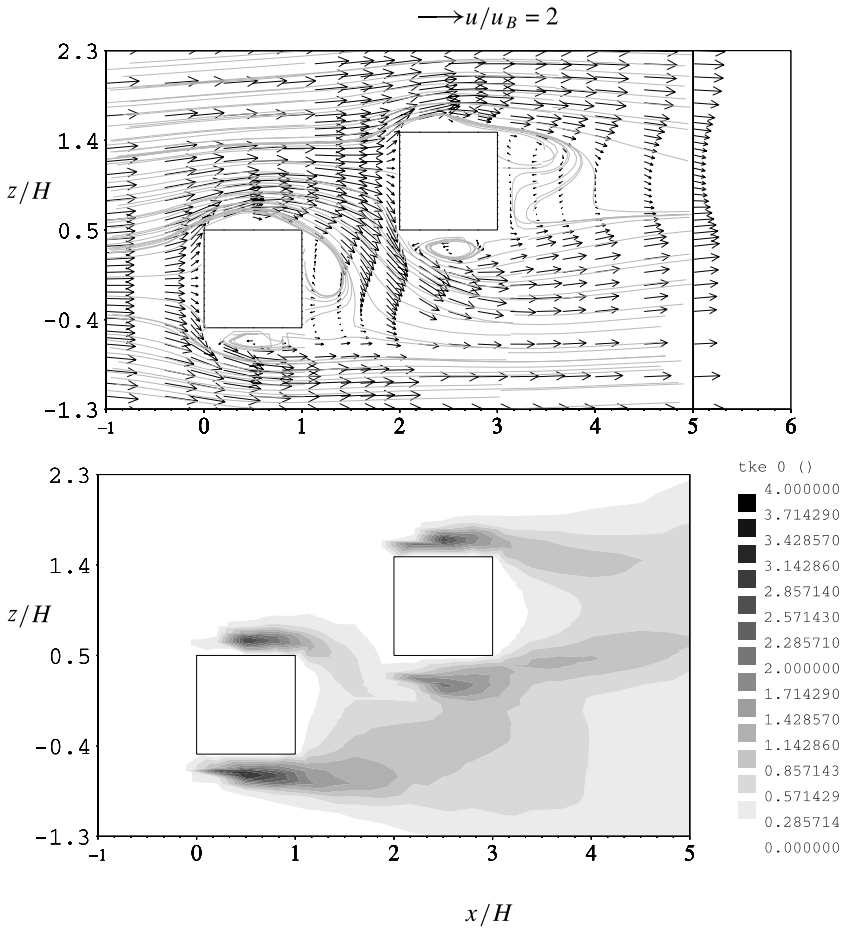

Fig. 9. Long-term averaged vector plot of the velocity field with streamlines (upper plot) and an iso-colour plot of the turbulent kinetic energy (lower plot) in a plane parallel to the channel floor at $y/H = 0.5$ for the off-axis tandem with $S_x/H = 2$ and $S_z/H = 1$ ($Re_H = 3900$).

The influence of the downstream cube on the time-averaged flow field diminishes for a larger streamwise distance. This can clearly be seen from the measurements for a tandem with a larger streamwise distance ($S_x/H = 4$) but the same spanwise distance ($S_z/H = 1$), see Fig. 10. The flow around the leading cube is almost unaffected by the downstream cube. The flow is rather symmetric in the plane $z/H = 0$ and resembles more or less an in-line tandem situation. The flow acceleration in the corridor between the cubes was less strong but still observable. The curvature associated with this corridor flow caused flow reattachment at the inner side face of the downstream cube. From the vector plot it is concluded that no flow reattachment occurred at the inner side face of the leading cube and outer side face of the downstream cube, but instead, the flow recirculations enveloped the entire face. Further, the protruding shape of the leading cube and the induced flow instabilities caused the wake flow to be highly turbulent, which caused smaller flow recirculations around the downstream cube, as is seen in Fig. 10.

While the plot of the turbulent kinetic energy is more or less symmetric for the upstream cube (see the iso-value plot of k in Fig. 10), a slightly increased turbulent intensity is observed at the inner side of the second cube. This was caused by the interaction with the extension of the upstream horseshoe vortex.

When the spanwise distance is increased to $S_z/H = 2$, with an unchanged streamwise distance $S_x/H = 4$, the situation becomes, as expected, more symmetric. This is observed from the LDA results given in Fig. 11.

4. Convective heat transfer

The heat transfer measurements were performed at $Re_H = 3900$. For the in-line tandems, the streamwise distance S_x/H was varied between $S_x/H = 0.5$ and ∞

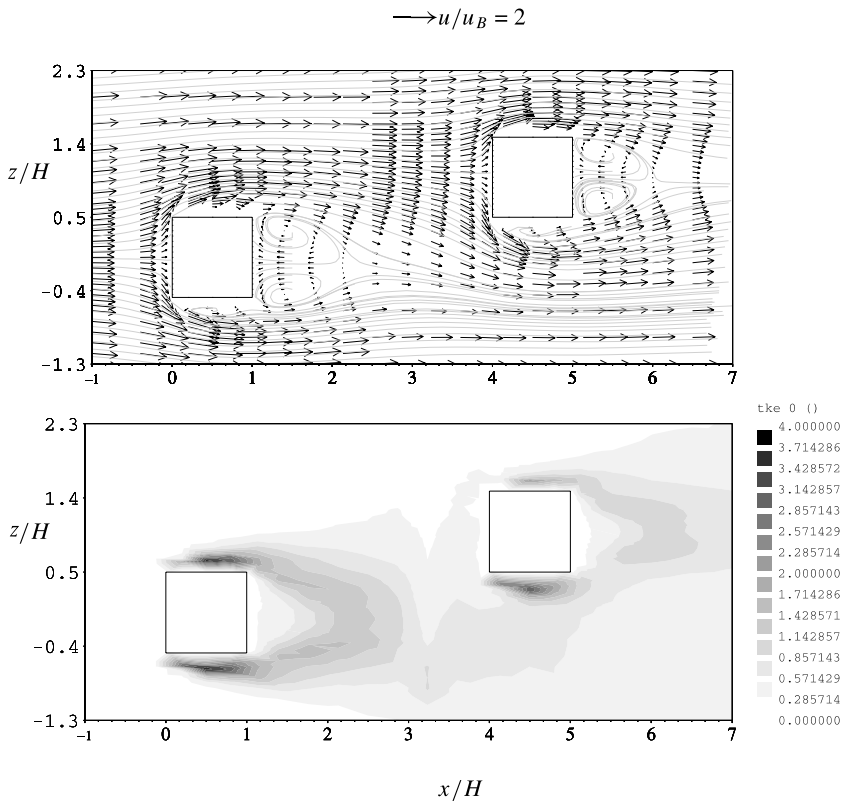

Fig. 10. Long-term averaged vector plot of the velocity field with streamlines (upper plot) and an iso-colour plot of the turbulent kinetic energy (lower plot) in a plane parallel to the channel floor at $y/H = 0.5$ for the off-axis tandem with $S_x/H = 4$ and $S_z/H = 1$ ($Re_H = 3900$).

while the spanwise distance was kept at zero ($S_z/H = 0$). Heat transfer measurements for the off-axis tandem were performed for a large series of streamwise and spanwise distances, i.e. $S_x/H = 2$ and $S_z/H = 0.5$, 1, 1.5, 2 and 3; $S_x/H = 4$ and $S_z/H = 0.5$, 1, 1.5, 2 and 3; $S_x/H = 8$ and $S_z/H = 0.5$, 1, 1.5, 2 and 3. Both cubes were separately powered to enable the use of the inlet flow temperature as the reference temperature. If both cubes were powered, the effect of upstream heating needed to be taken into account which involved a different experiment to determine the actual adiabatic temperature of the cube in question [7]. Again, the distinction between the inner and outer side face of the leading and the downstream cube is made (see Fig. 1).

4.1. In-line tandem

4.1.1. Distributions of the local convective heat transfer

Distributions of the heat transfer coefficient for the leading cube in the in-line tandem, given in Fig. 12 for $S_x/H = 2$, 4 and 8, are shown along two paths: path *ABCDA* denotes a plane parallel to the channel floor at half a cube height $y/H = 0.5$; path *ABCD* denotes a plane perpendicular to the channel floor at $z/H = 0.5$. It is noted that the h profiles are symmetric around the plane of symmetry, indicated with the dotted lines in the upper plot in Fig. 12.

Although a large spatial variation in the local heat transfer coefficient is observed, the differences between the results for the different in-line cases ($S_x/H = 2$, 4 and 8) are very small. The profiles of the heat transfer coefficient at the top and side faces show a distinct minimum and maximum, located at the front half and the back half of these faces, respectively. For all three values of S_x/H, a vortex was observed to exist at the side faces and a bound vortex on the top of the cube. The heat removed from the hot cube faces was re-entrapped by the vortex and caused the local fluid temperature to increase. As a consequence, the convective heat transfer decreased, which led to the observed minimum in h. The intermittent reattachment of the cold shear layer close to the trailing edges favoured the convective heat transfer.

From the previous discussion of the local flow measurements it can be concluded that only minor differences existed in the flow structure in the vicinity of the leading cube. The distributions of the heat transfer co-

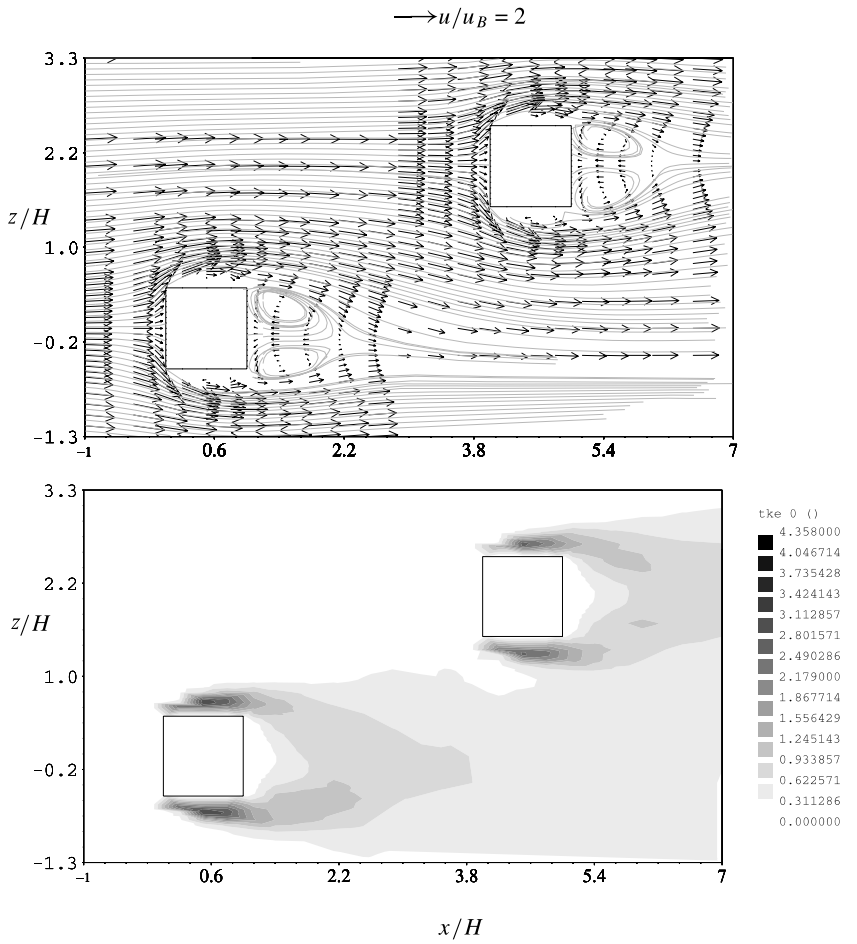

Fig. 11. Long-term averaged vector plot of the velocity field with streamlines (upper plot) and an iso-colour plot of the turbulent kinetic energy (lower plot) in a plane parallel to the channel floor at $y/H = 0.5$ for the off-axis tandem with $S_x/H = 4$ and $S_z/H = 2$ ($Re_H = 3900$).

efficients for $S_x/H = 2$, 4 and 8 support this conclusion. Heat transfer coefficient distributions along path *ABCDA* of the second cube in the in-line tandem arrangement are given in Fig. 13 for different streamwise distances S_x/H. It is seen from the figures that the convective heat transfer at the back face is hardly affected by a variation in S_x/H. This is expected since it appeared from the flow measurements that the wake vortex of the second cube was rather similar in size for all the considered in-line tandems. The h profiles at the front face of the downstream cube have a more or less concave shape, in particular for the smaller streamwise spacings. Such a shape in the local heat transfer coefficient was also found for the front face of the downstream cubes in the in-line row, see [6]. It was explained that the concave shape was caused by the counter-rotating extensions of the arch-shaped vortex in the inter-obstacle spacing. The local heat transfer coefficient at the side faces is quite different for the different streamwise spacings. For the smallest spacing considered, $S_x/H = 2$, h decays monotonically in the downstream direction. The separated shear layer from the leading cube reattached at the front edges with the absence of a flow recirculation. The gradual decrease in h is explained by the resulting boundary layer flow: heat convection from the hot surfaces heats up the local air flow. The increase in fluid temperature subsequently causes a reduction in the downstream surface heat flux. When the streamwise distance is increased to $S_x/H = 4$, a small vortex appears at the side faces close to the leading edge (see Fig. 4). The rotational flow in this rather small vortex caused the local minimum in the heat transfer coefficient, close to the leading edge. The flow reattachment downstream at the side face caused a small increase in h. An examination of the convective heat transfer for the intermediate distances shows the gradual transition from h distributions caused by boundary layer flow to h distributions caused by the flow recirculations.

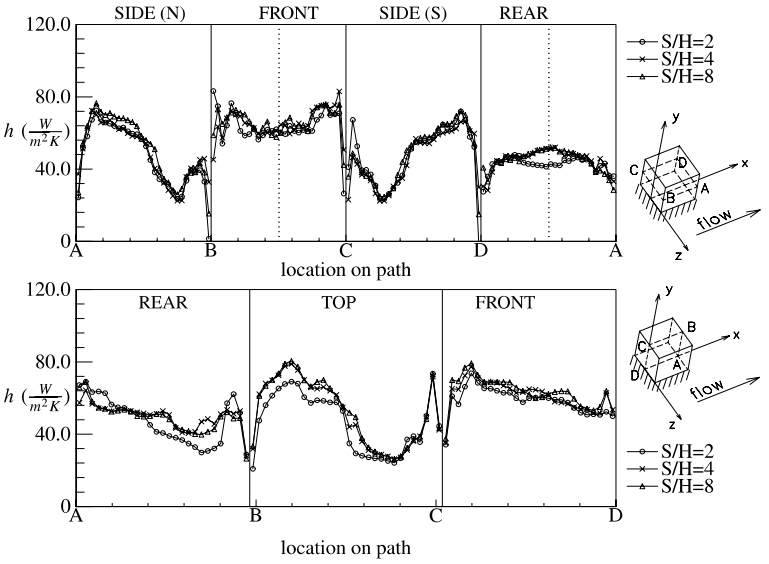

Fig. 12. Heat transfer coefficient distributions along path *ABCDA* (upper plot) and along path *ABCD* (lower plot) for the leading cube in the in-line tandem as a function of S_x/H.

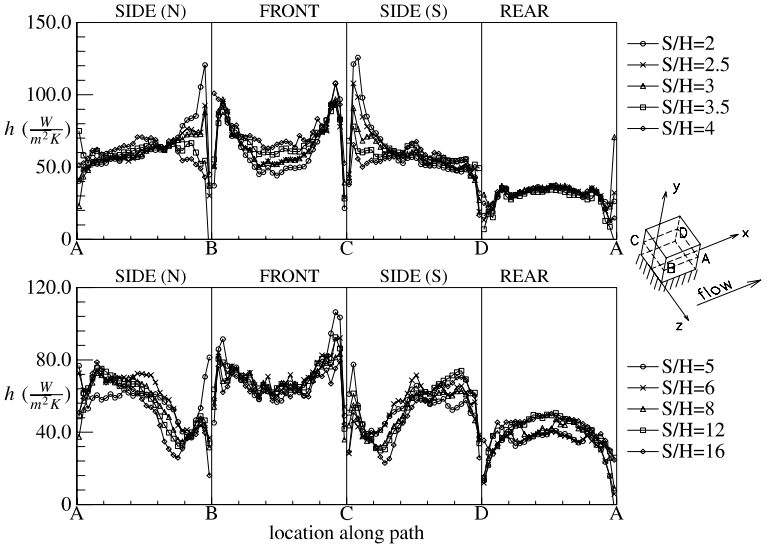

Fig. 13. Heat transfer coefficient distributions along path *ABCDA* for the second cube in the in-line tandem as a function of S_x/H. The upper figure shows the results for $S_x/H = 2$, 2.5, 3, 3.5 and 4. The lower figure refers to $S_x/H = 5$, 6, 8, 12 and 16.

For larger distances, the side vortex increased in size and strength. This is reflected in the more pronounced heat transfer minima and maxima. It was shown from the flow measurements that the flow structure around the upstream and downstream cube was similar for $S_x/H = 8$ and larger. This is in agreement with the observation that the distributions of h are qualitatively similar to those of the leading cube, see Fig. 12.

The distributions of h along a cross-section perpendicular to the channel floor, path *ABCD*, are shown in Fig. 14. Again the heat transfer characteristics at the back face hardly depend on S_x/H. The transition from convective heat transfer caused by boundary layer flow, for $S_x/H = 2$, to a situation in which the heat transfer is dominated by the bound vortex on top of the obstacle, for $S_x/H > 4$, is obvious from the distributions. The

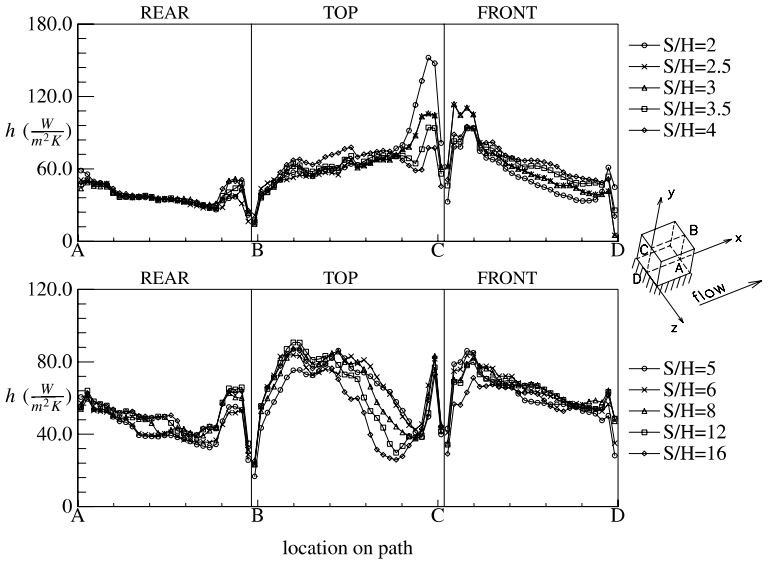

Fig. 14. Heat transfer coefficient distributions along path *ABCD* for the second cube in the in-line tandem as a function of S_x/H. The upper figure shows the results for $S_x/H = 2$, 2.5, 3, 3.5 and 4. The lower figure refers to $S_x/H = 5$, 6, 8, 12 and 16.

marked minimum at the lower edge of the front face is caused by the flow recirculation in the inter-obstacle space. For $S_x/H = 2$, a recirculation in the cavity caused a gradual decrease towards the lower edge (towards *D*). The development of a horseshoe vortex for the intermediate spacings $S_x/H = 4$ resulted in the pronounced minimum close to the channel wall. The heat convected from the cube surface recirculated in the vortex and caused the local fluid temperature to be elevated.

The aforementioned differences in the local convective heat transfer for the various distances S_x/H studied can be observed from the folded-out isotherm maps of the surface temperature distributions for the five faces of the cube, as given in Fig. 15. The plots show a qualitatively similar temperature pattern for the front and back face for all values of S_x/H. For these faces, it is noted that for the larger distances fewer isotherms are shown due to the high temperature levels at the other faces. Substantial differences between the isotherm patterns of the small and large distances S_x/H are observed at the side and the top faces.

4.1.2. Time-dependent convective heat transfer

It appeared from the flow study that variation of S_x/H had a significant effect on the flow structure around the downstream cube while the flow pattern around the leading cube was only a little affected. For $S_x/H = 2$, the separated shear layer reattached more or less at the side edge of the downstream cube; it reattached in the inter-obstacle spacing at about $x/H = 2.5$ for $S_x/H = 4$ and larger. The flow structure around the upstream and downstream cube was more or

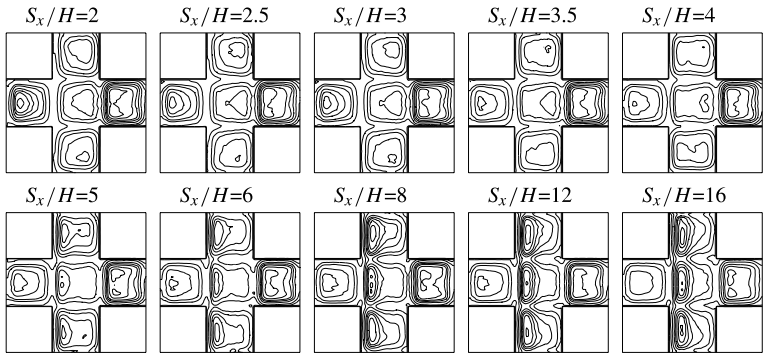

Fig. 15. Isotherm maps of the surface temperature of the second cube in the in-line tandem arrangement for various values of S_x/H. Flow is from left to right.

less similar for $S_x/H > 8$. The wake flow of the upstream cube showed oscillatory behaviour due to the shed vortices behind its side faces. The frequency of vortex shedding was modulated by the aerodynamic interaction with the downstream cube resulting in a dependency on the streamwise distance S_x/H. The vortex shedding frequency was minimum for $S_x/H = 2.9$. Dependent on S_x/H, the shed vortices reattach more or less periodically at the side faces of the downstream cube, presumably causing the time-dependent heat flux to fluctuate also periodically. This coupling was demonstrated for geometries other than wall-mounted cubes [11–14] and, therefore, expected in this case to be present as well.

Measurements of the time-resolved convective heat flux were performed with an active heat-flux sensor. The sensor consisted of a rectangular glass substrate of size 10×4 mm. Two metal pins were melted in the glass substrate at a distance of 4 mm apart in a parallel orientation. A thin platinum film of thickness 0.2 μm was vapour deposited on the glass substrate. This resulted in an active sensor area of size 4×4 mm. The metallic connectors embedded in the glass substrate acted as current spreaders to obtain a uniform electric current distribution throughout, and thus uniform heat-flux distribution in the platinum film. The electrical resistance of the thin platinum film was temperature-dependent. The sensor was connected to a Wheatstone bridge of a conventional hot-wire controller. The electrical power to the sensor was adjusted such that the temperature of the metal sheet remained constant. The used electrical power is then directly proportional to the heat transfer from the hot film.

The output voltage of the hot-film controller was sampled with a signal memory recorder. The sample frequency was between 300 and 500 Hz, which is sufficiently large compared to the vortex shedding frequencies in question. The number of data points for one measurement was about 32,000.

The absolute value of the heat flux signal was not calibrated because of the time-dependent heat losses, which were rather large but difficult to estimate correctly. Since we were only interested in the frequency information contained by the time-dependent convective heat flux, we performed two dynamic calibrations to ensure an accurate frequency response up to at least 200 Hz. One calibration is based on a modulated laser beam focused on the sensor, chopped with a known frequency. In the other dynamic calibration, the sensor was located in the wake of a cylinder with known vortex shedding behaviour. In both cases, the predominant frequencies were determined from power density spectra of the measured sensor response signal. These calibrations are elaborated in more detail in [7].

The sensor was mounted flush in the side face of a cube of formaldehyde. Formaldehyde was chosen since it was easy to machine and it had a low thermal conductivity of $\lambda = 0.33$ W m^{-1} K^{-1}. The location of the sensor was selected such that the frequency response was optimum.

Simultaneously, a hot-wire anemometer was used to measure the spanwise velocity in the wake of the upstream cube. The vortex shedding frequency was then obtained from the corresponding power density spectra. Standard numerical recipes with windowing were used to calculate the spectra. A cross-spectrum of both the heat flux and the velocity signal is shown in Fig. 16 for a typical experiment. The streamwise distance was $S_x/H = 3$, and the bulk velocity was $u_B = 2$ m s^{-1}. A marked peak is found at $f = 8 \pm 1$ Hz, which corresponds to a Strouhal number of $St = 0.06$. Apparently, the periodic flow reattachment at the sides of the downstream cube causes the time-dependent heat flux to fluctuate periodically as well.

The Strouhal number of $St = 0.06$ is in good agreement with the results given in Fig. 7 for the tandem of two cubes in the fully developed turbulent channel flow. These results are reproduced in Fig. 17. The Strouhal

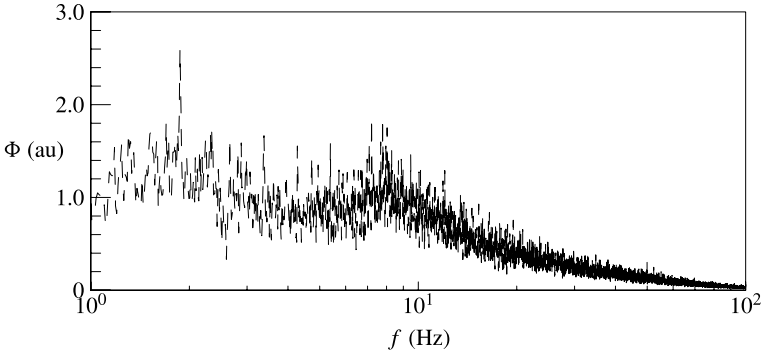

Fig. 16. Spectrum of the cross-correlation between the time-dependent heat flux and the velocity signal at the side face of the downstream cube in the in-line tandem for $S_x/H = 3$ and $Re_H = 2000$.

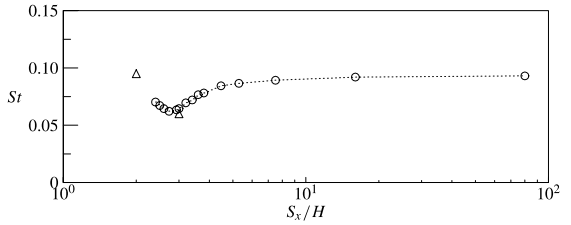

Fig. 17. Dominant wake frequencies of the leading cube as a function of S_x/H for the in-line tandem in the fully developed turbulent channel flow. LDA measurements of the vortex shedding are indicated with (○), the dominant frequencies in the heat flux signal are indicated with (△).

number obtained with the heat flux sensor is indicated with (△) for $S_x/H = 3$.

A periodic heat flux is only present when the sensor is subject to oscillatory flow, which is only the case for some combinations of S_x/H and the bulk velocity. A distinguishable peak was also observed for $S_x/H = 2$ and $u_B = 1.9$ m s^{-1}. The Strouhal number for this case was $St = 0.095$. This value is also in good agreement with shedding frequency results, as shown in Fig. 17.

The noise level in the hot-wire signals was rather high due to the limited number of samples used to calculate the spectrum. Further, the hot-wire probe was positioned in an area where the amplitude of the oscillating flow was small. Since the vortex shedding frequency was clear from the spectrum, we did not attempt to improve the signal-to-noise ratio. The sensor area was not infinitely small but 4×4 mm^2, which caused a spatial averaging of the event.

4.1.3. Averaged heat transfer coefficients

The face-averaged heat transfer coefficients $\bar{h}$ were calculated from the face-averaged convective heat flux and surface temperature. Results for various streamwise distances S_x/H are given in Fig. 18. The side and top faces exhibit a small minimum in $\bar{h}$ around $S_x/H = 3$, which is the location at which the shedding frequency is minimum as well. Since the side and top vortices, induced by the upstream cube, reattach at the corresponding faces of the downstream cube, and augment the heat transfer in that way, it is plausible that the minima in $\bar{h}$ are correlated to the shedding frequency of these vortices. It is noted that the causality between the minima in shedding frequency and convective heat transfer is weak. The face-averaged heat transfer at the front and back face is more or less constant around $S_x/H = 3$. The cube-averaged heat transfer coefficient, determined from the cube-averaged heat flux and surface temperature, shows also a small minimum around $S_x/H = 3$. Apparently, the side and top faces contribute markedly to the cube-averaged heat transfer. The dip in $\bar{h}$ at $S_x/H = 5$ is explained by a temporary reduction of the averaged flow rate. If we consider the total supplied power P (the product of the voltage and current) we indeed see a deviation at $S_x/H = 5$, see Fig. 19. The second measurement series of the supplied power, obtained from an independent measurement and indicated with (△) in Fig. 19, shows a monotonic increase up to $S_x/H = 6$, indicating that the local minimum around $S_x/H = 5$ is an experimental artifact. Fig. 19 further shows a realistic minimum in the supplied power around $S_x/H = 3$, which supports the hypothesis that the shed vortices interact locally with the surface.

In general, the variations in the face-averaged and cube-averaged heat transfer coefficient as a function of S_x/H are rather small compared to the variations in the local heat transfer coefficient. Besides the minimum around $S_x/H = 3$, the only marked variation is found at the leeward face for which $\bar{h}$ increases slightly with increasing distances. The averaged heat transfer coefficient for the other faces decreases slightly.

4.2. Off-axis tandem

4.2.1. Distributions of the local heat transfer coefficient

Because the local heat transfer characteristics and their associated flow features were already discussed in

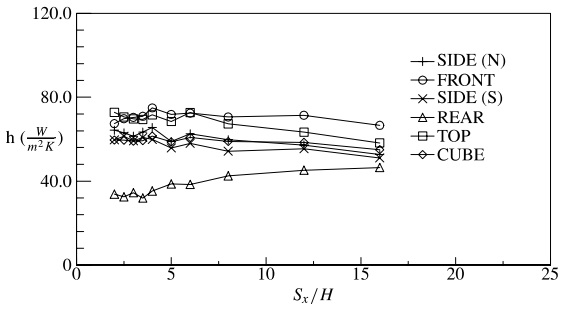

Fig. 18. Spatially averaged heat transfer coefficients as a function of S_x/H for the second cube in the in-line tandem: (+) side (north), (○) front, (×) side (south), (△) rear, (□) top and (◇) cube average.

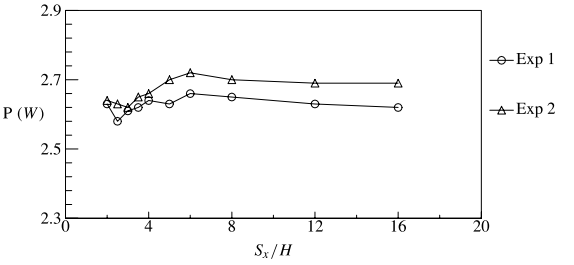

Fig. 19. Total supplied power as a function of S_x/H for the in-line tandem configuration. The different markers denote different experiments.

detail for the in-line tandem, the discussion in this section will primarily be on the asymmetry of the local convective heat transfer. Significant asymmetry effects were observed when both cubes were positioned close together, i.e. for small values of S_x/H and S_z/H. Profiles of the local heat transfer coefficient are given in Fig. 20 along paths *ABCDA* and *ABCD* for the downstream cube in a typical off-axis arrangements with severe asymmetry effects, i.e. $S_x/H = 2$ and $S_z/H = 0.5$. The dotted lines refer to the centreline of the cube and denote a possible symmetry plane ($x/H = 0.5$). It is seen that the profiles are significantly asymmetric. The flow acceleration through the corridor between the two cubes caused the distinct peak in h at the front face. This flow acceleration was observed for $S_x/H = 2$ and $S_z/H = 1$ (see Fig. 9), but it is more pronounced for smaller spanwise distances. The inner side face of the downstream cube, indicated with *CD* in the upper plot in Fig. 20, shows a marked minimum close to the leading edge, caused by the side vortex. The maximum located at the middle of this side face is due to flow reattachment. The heat transfer coefficient profiles at the outer side are caused by the flow recirculation which enveloped almost the entire face. The convective heat transfer at the back face of the downstream cube decays monotonically towards the outer side face of the cube which is opposite to the local air speed of the rotating wake vortex. The heat removal from the surface caused an increase in the fluid temperature and, therefore, reduced the convective heat transfer. The top face (shown in the lower plot in Fig. 20) exhibits more or less similar heat transfer features as for the single cube. The heat transfer coefficient decays strongly up to approximately $x/H = 1/4$, where a local minimum is found. This is the location of the top vortex. The subsequent flow reattachment caused the heat transfer to become maximum at about $x/H = 1/2$.

4.2.2. Average heat transfer

The local convective heat transfer appeared to be strongly correlated to the local flow structure in the proximity of the cubes. Even face-averaged heat transfer coefficients showed significant differences for the different off-axis situations considered (this is not further discussed here). But if we plot all the measured cube-averaged heat transfer coefficients for the downstream cube in the off-axis tandem as a function of the streamwise distance S_x/H, the results coincide pretty well. This can be seen in Fig. 21, in which the different markers refer to different spanwise distances S_z/H. The results for $S_z/H = 0$, the in-line tandem arrangements, are also included in the figure. All results were obtained for $Re_H = 3900$. The solid line refers to a cube-averaged heat transfer coefficient of $h = 59$ W m^{-2} K^{-1}. The dashed lines indicate a bandwidth of 5% experimental uncertainty. The scatter is remarkably small, which suggests that the overall cooling of the cube is dominated by the bulk flow. Although severe differences were observed in the distributions of the local heat transfer coefficient, the cube-averaged heat transfer coefficient apparently is not a function of the location of this cube with respect to its upstream neighbour. A similar observation was already made for the leading cube.

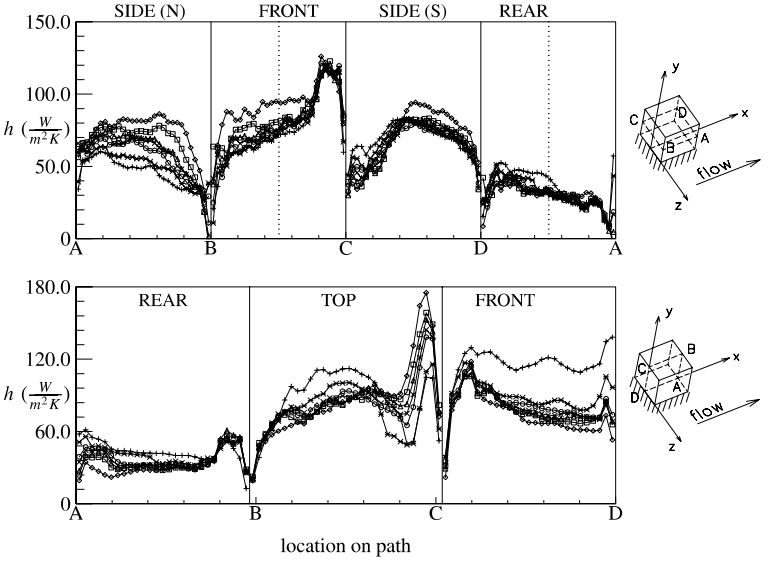

Fig. 20. Heat transfer coefficient distributions along path *ABCD* (upper plot) and along path *ABCDA* (lower plot) for the downstream cube in the staggered tandem for $S_x/H = 2$ and $S_z/H = 0.5$. The different symbols refer to different locations of the cross-sections.

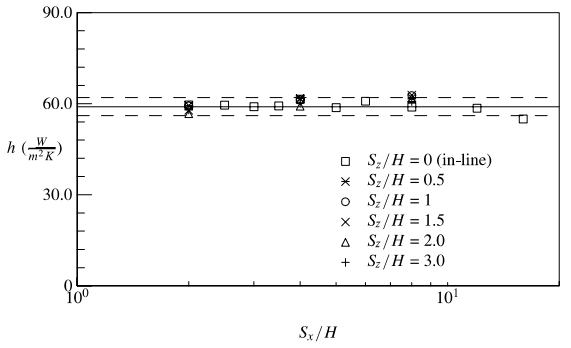

Fig. 21. Cube-averaged heat transfer coefficient for different spanwise distances S_z/H as a function of the streamwise distance S_x/H. The solid line indicates the averaged value of $\bar{h} = 59$ W m^{-2} K^{-1}, the dashed lines indicate an uncertainty range of 5%.

5. Conclusions

Experimental study of flow field, turbulence and local heat transfer from two wall-mounted heated cubes, placed in in-line and staggered arrangement, revealed some striking similarities, but also some basic differences. In both cases, the longitudinal spacing is the crucial parameter that influences the flow pattern, especially between the cubes and, consequently, the heat transfer on both cubes.

For the in-line configuration, the variation of the streamwise distance S_x/H had a significant effect on the local flow structure around the downstream cube. It varied gradually from shear layer flow, for small streamwise distances, to flow separation at the top and side faces, for sufficiently large streamwise spacings. On the other hand, the flow around the leading cube was hardly affected. It was characterised by a complex vortex system which typically included the horseshoe vortex, the top, side and wake vortices.

The flow structure measured around the cubes in the off-axis tandem arrangement is qualitatively different due to flow blockage by the downstream cube, which causes a flow deflection and a pronounced asymmetry. This is especially noticeable at smaller longitudinal spacing, roughly for less than two cube sizes. However, the front of the leading cube remains to a large extent unaffected and symmetric for all arrangements considered. The distinct flow features, such as flow separation and reattachment, lead to marked differences in the distribution of the local convective heat transfer. Only for the staggered tandem arrangements with small values of S_x/H and S_z/H were significant asymmetric flow structures observed which lead to an asymmetric distribution of the local convective heat transfer as well.

The time-dependent convective heat transfer was measured with a fast-responding active heat flux sensor. The wake flow of the upstream cube was subjected to flow periodicities caused by vortex shedding. Dependent on S_x/H, the periodically oscillating shear layer reatached on the side faces of the downstream cube, causing the convective heat flux to vary periodically as well. This was demonstrated from power density spectra of the heat flux signal while the vortex shedding frequency was simultaneously measured with a hot-wire anemometer. These results were in good agreement with the LDA frequency measurements.

Although large differences were found in the distributions of the local heat transfer coefficient for the different in-line and staggered tandem arrangements, the cube-averaged heat transfer coefficients appeared to be insensitive to both the streamwise and spanwise distance between the cubes. This suggests that primarily the bulk flow through the channel dictates the overall convective heat transfer from the cubes.

Acknowledgements

Most of the work was performed at the Applied Physics Department of the Delft University of Technology. The work was financially supported by Philips, Nederlandse Philips Bedrijven B.V., The Netherlands. E.R. Meinders obtained financial support from The Netherlands Organisation for Scientific Research (NWO) to perform preliminary research at The University of Western Ontario, London, Canada and at The University of Arizona, Tucson, US. A. Ortega of The University of Arizona, Tucson, is acknowledged for discussions.

References

[1] R.J. Martinuzzi, C. Tropea, The flow around surface-mounted prismatic obstacles placed in a fully developed channel flow, J. Fluids Eng. 115 (1993) 85–92.
[2] T. Takeuchi, Effects of geometrical shape on vortex-induced oscillations of bridge tower, J. Wind Eng. Ind. Aerodyn. 33 (1990) 359–368.
[3] T. Takeuchi, M. Matsumoto, Aerodynamic response characteristics of rectangular cylinders in tandem arrangement, J. Wind Eng. Ind. Aerodyn. 41–44 (1992) 565–576.
[4] R. Devarakonda, J.A.C. Humphrey, Experimental study of turbulent flow in the near wake of single and tandem prisms, Int. J. Heat Fluid Flow 17 (1996) 219–227.
[5] S.C. Luo, T.C. Teng, Aerodynamic forces on a square section cylinder that is downstream to an identical cylinder, Aeronaut. J. (1990) 203–212.
[6] E.R. Meinders, T.H. van der Meer, K. Hanjalić, Local convective heat transfer from an array of wall-mounted cubes, Int. J. Heat Mass Transfer 41 (2) (1998) 335–346.
[7] E.R. Meinders, Experimental study of heat transfer in turbulent flows over wall-mounted cubes, Ph.D. thesis,

Faculty of Applied Sciences, Delft University of Technology, Delft, Netherlands, 1998.

[8] E.R. Meinders, K. Hanjalić, Vortex structure and heat transfer in turbulent flow over a wall-mounted matrix of cubes, Int. J. Heat Fluid Flow 20 (3) (1999) 255–267.

[9] E.R. Meinders, K. Hanjalić, R.J. Martinuzzi, Experimental study of the local convective heat transfer from a wall-mounted cube in turbulent channel flow, J. Heat Transfer 121 (3) (1999) 564–573.

[10] E.R. Meinders, G.M.P. van Kempen, L.J. van Vliet, T.H. van der Meer, Measurement and application of an infrared image restoration filter to improve the accuracy of surface temperature measurements of cubes, Exp. Fluids 26 (1–2) (1999) 86–96.

[11] J.W. Scholten, D.B. Murray, Unsteady heat transfer and velocity of a cylinder in cross-flow – I. Low free stream turbulence, Int. J. Heat Mass Transfer 41 (10) (1998) 1139–1148.

[12] J.W. Scholten, D.B. Murray, Unsteady heat transfer and velocity of a cylinder in cross-flow – II. High free stream turbulence, Int. J. Heat Mass Transfer 41 (10) (1998) 1149–1156.

[13] S.G. Simmons, J.M. Hager, T.E. Diller, Simultaneous measurements of time-resolved surface heat flux and free stream turbulence at a stagnation point, in: G. Hetstroni (Ed.), Proceedings, Heat Transfer, vol. 2, Hemisphere, New York, 1990, pp. 375–380.

[14] T. Mancuso, T.E. Diller, Time-resolved heat flux measurements in unsteady flow, in: Proceedings, Fundamental Experimental Measurement in Heat Transfer, ASME, New York, 1991, pp. 67–74.